III−V Nitride Epilayers for Photoelectrochemical Water Splitting: GaPN and GaAsPN†

Todd G. Deutsch,‡ Carl A. Koval,§ and John A. Turner*,‡

National Renewable Energy Laboratory, 1617 Cole Boulevard, Golden, Colorado 80401 and Department of Chemistry & Biochemistry, University of Colorado, 215 UCB, Boulder, Colorado 80309

Received: August 15, 2006; In Final Form: October 9, 2006

Epilayers of single-crystal GaAsPN and GaPN semiconductor samples with varying nitrogen compositions were photoelectrochemically characterized to determine their potential to serve as water splitting photoelectrodes. The band gap and flatband potentials were determined and used to calculate the valence and conduction band edge energies. The band edges for all compositions appear to be too negative by more than 500 mV for any of the materials to effect light-driven water splitting without an external bias. Corrosion analysis was used to establish material stability under operating conditions. GaPN was found to show good stability toward photocorrosion; on the other hand, GaAsPN showed enhanced photocorrosion as compared to GaP.

Introduction

For a semiconductor material to photoelectrochemically split water it must satisfy several main criteria. (i) The band gap must be a minimum of ∼1.7 eV to provide the potential necessary for electrolysis and overcome other energy losses in the system.[1] (ii) The minority band edge and the Fermi level of the material must straddle the hydrogen and oxygen redox potentials for current to flow through the circuit. (iii) The material must be stable in contact with the electrolyte and (iv) have high efficiency in the conversion of photons to separated electron/hole pairs. (v) Additionally, charge transfer at the interface must be fast enough to prevent accumulation of minority carriers at the semiconductor surface that can shift the band edges out of the overlap position. These necessary criteria must all be met simultaneously, and even then, efficient water splitting is not guaranteed. To date, no suitable material has been identified.

Photovoltaic devices composed of III−V materials have the highest conversion efficiency of any solar conversion system. However, when used in photoelectrochemistry these materials show very short lifetimes due to photocorrosion. A nontraditional III−V that shows excellent stability as a PEC device is GaN. It has been characterized,[2,3] and its band edges meet the energetic overlap condition, the only known single junction III−V that does. Its stability is a property rarely observed in III−V semiconductors. Although direct, the band gap at 3.4 eV is too wide for terrestrial solar applications; it absorbs only in the UV, leading to low photoelectrolysis efficiency. Another nontraditional III−V, GaP has been reported to have a relatively small band edge mismatch with the water splitting reaction as compared to other III−V alloys, with its valence band edge around 300 mV too negative to meet the overlap requirement.[4] Moreover, the band gap is still too wide at 2.26 eV; it has an indirect transition, making GaP an inefficient absorber of solar radiation,[4] and GaP showed insufficient stability in solution. A mixed alloy of Ga−P−N might have the right combination of properties to enable water photoelectrolysis. Addition of nitrogen to GaP actually results in the *lowering* of the band gap via a phenomenon known as band gap bowing.[5] Another beneficial result of nitrogen addition is the transformation of the band gap of GaP from an indirect to a direct transition in the relatively dilute nitrogen regime. Literature reports that the observed crossover to direct transition occurs below 0.5% nitrogen (at. % of group V elements).[6]

GaPN can be grown via metal organic chemical vapor deposition (MOCVD) or molecular beam epitaxy (MBE) using commercially available GaP wafers as substrates. Nitrogen incorporation into the GaP lattice decreases the epilayer lattice constant. This results in a lattice mismatch with the GaP substrate, a consequence of which is the creation of misfit dislocations that can act as nonradiative recombination centers, lowering the quantum efficiency of the material.[7] The strain in the crystal structure can also change the electronic band structure due to loss of symmetry.[8] One can easily predict that epilayers of GaPN would quickly become lattice mismatched from the GaP substrates unless a lattice-expanding constituent is added to balance the contracting effect of nitrogen. By adding arsenic along with nitrogen, the lattice constant decrease from nitrogen can be compensated for by an increase in the lattice constant from the arsenic. From this, a higher nitrogen-containing composition of $GaAs_yP_{1-x-y}N_x$ that is lattice matched to the GaP substrate can be realized. Vegard's law indicates that this alloy will be lattice matched when $y = 4.7x$.[7]

GaAsPN has been examined for use in solar cells, and a number of characteristics were noted: photodoping was one unique characteristic. Geisz et al. found that the free carrier concentration increased as the light bias was increased.[9] Depending on the growth conditions, impurity concentrations of both hydrogen and carbon range from the SIMS limit of detection (1×10^{17} cm^{-3}) up to 1×10^{20} cm^{-3}.[10] This is an undesirable property in the current GaAsPN films as impurities diminish the performance of solid-state devices by creating defect sites. To date, the performance of GaAsPN photovoltaic devices has been mediocre due to poor minority carrier transport.[11] Nonetheless, GaPN and GaAsPN are of interest to determine their energetics and the influence of arsenic and nitrogen on the corrosion properties. Photoelectrochemical

† Part of the special issue "Arthur J. Nozik Festschrift".

* To whom correspondence should be addressed. Phone: 303-275-4270. Fax: 303-275-2905. E-mail: John_Turner@nrel.gov.

‡ National Renewable Energy Laboratory.

§ University of Colorado.

10.1021/jp0652805 CCC: $33.50
Published on Web 12/14/2006

characterization and corrosion analysis was accomplished on an array of GaPN and GaAsPN epilayers to determine, semi-quantitatively, the influence of nitrogen on interfacial energetics and material durability.

Experimental Methods

Epilayers of GaPN (1 μm) and GaAsPN (1 or 2 μm) were grown, without intentional addition of dopants, by atmospheric-pressure MOCVD on heavily zinc-doped (001) GaP substrates. The growth rate was 1 μm/h at 700 °C, which was determined to be the optimum temperature to minimize carbon and hydrogen contamination.[12] The feedstock gases were triethylgallium, unsymmetric dimethylhydrazine, phosphine, and *tert*-butylarsine with hydrogen as the carrier gas. Ohmic back contacts were made by electron beaming palladium, followed by electroplating zinc, followed by another electron-beamed layer of palladium. The wafers were cleaved and mounted using previously published techniques[13] that left only the front surface of the semiconductor exposed to the environment.

Dilute amounts of nitrogen can have a large influence on electronic properties of the alloy, so an ideal composition might be achievable with a tolerable mismatch. With the expectation that the benefits of nitrogen incorporation might go through a local maximum before further addition compromised the crystallinity, 1 μm $GaP_{1-x}N_x$ epilayers were grown on GaP substrates with $0 \leq x \leq 0.035$. Samples with nitrogen content over 3.5% did not form a crystalline layer, which was taken as the upper limit of nitride composition accessible on GaP substrates. A few zinc-doped GaP epilayers were grown on the same substrate by MOCVD to serve as a control. A sample of $GaAs_{0.21}P_{0.89}$ was also grown to evaluate the influence of arsenic on GaP in the absence of nitrogen.

Photocurrent spectroscopy was accomplished using a three-electrode cell with the semiconductor as the working electrode, a platinum counter electrode ($\sim$5 cm^2), and an Ag/AgCl (SSC) reference electrode. The filling solution in the SSC electrode was 3 M NaCl, giving +0.206 V vs NHE. The electrolyte was 1 mM Hexaammineruthenium(III) chloride (Strem) in a buffer solution. The buffer solution was Hydrion pH 10 carbonate for GaAsPN and Hydrion pH 2 biphthalate for all GaPN sample configurations. The pH 10 buffer solution was initially chosen because GaAsPN showed a more ideal Mott−Schottky response in basic solutions. The Ru ion was unstable in pH 10, so pH 2 buffer was subsequently employed. The excitation source was a Photon Technology International (PTI) 100 W tungsten bulb connected to a PTI 102 dual-grating monochromator. The 1200 lines/mm 500 blaze grating with a slit width of 1.04 mm was used, giving rise to a resolution of the analysis to $\pm$0.01 eV. Light bias had a negligible influence on the photocurrent magnitude and was not employed for this study. A potential of −0.7 V vs the reference was applied by an EG&G Princeton Applied Research 263A potentiostat/galvanostat. The reverse bias was used to ensure adequate band bending to facilitate carrier collection. Changing the applied bias (in the reverse bias regime) had a moderate influence on the magnitude of measured photocurrent. Band gap determination is independent of photocurrent magnitude because the linearity and x intercept are preserved. Light exiting the monochromator was chopped at 37 Hz, and an optical filter was used to block any second-order diffraction. The signal was detected using a Stanford Research Systems model SR830 DSP lock-in amplifier using the chopping frequency as a reference. Data was collected on a PC running LabVIEW. The spectral output of the lamp and monochromator was measured using a thermopile detector in place of the electrochemical cell; the chopping frequency was 7 Hz.

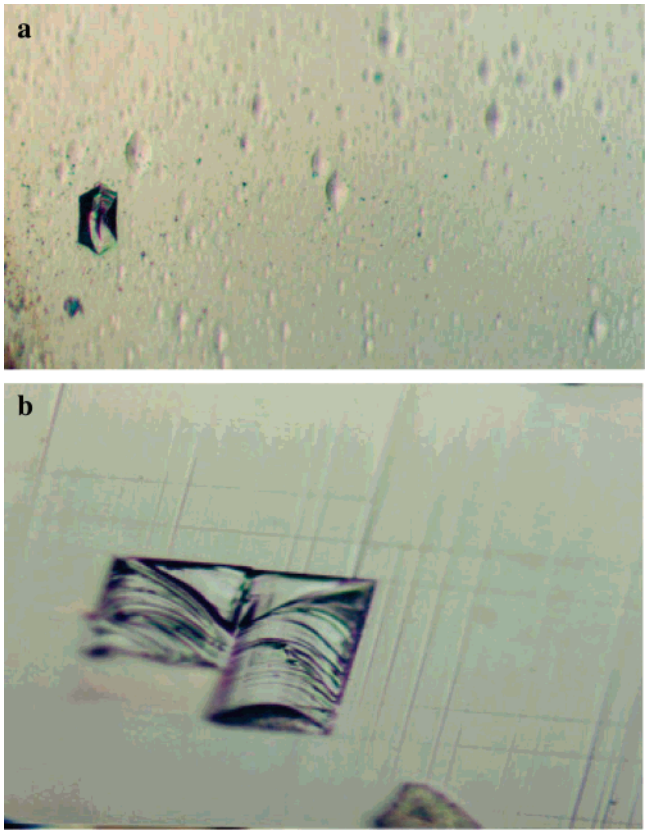

Figure 1. Optical microscopic images (400×) of (a) point defects in GaAsPN (3.6% N) and (b) crosshatches around a surface defect region of highly lattice mismatched GaPN (3.5% N). The crosshatches appeared on the surfaces of epilayers with nitrogen concentrations greater than 1.6%.

The output from the thermopile is a voltage proportional to incident radiation power, which was plotted vs photon energy. To convert this spectrum to a photon flux, the photocurrent signal at each wavelength was divided by the energy (eV) of that wavelength. The result was a relative flux of photons at each wavelength. The semiconductor photocurrent spectrum was divided by the photon flux spectra to get a normalized, corrected photocurrent.

Current−potential curves were taken with a Solartron SI 1287 Electrochemical Interface potentiostat controlled by a PC running a Scribner Associates International (SAI) Corrware program and analyzed using Corrview software from the same vendor. The scan rates were 25 mV/s. The broadband illumination source was a Cole Parmer model 41500-50 fiber optic illuminator equipped with a 150-Watt tungsten−halogen bulb. Initial illumination intensity measurements were made using a Scientech Astral AD30 optical power meter equipped with a thermopile detector. The readout from this meter is in mW/cm^2, and illumination intensities denoted as "1 sun" correspond to 100 mW/cm^2. Further into the investigation, illumination intensity was measured using a 1.986 eV GaPN reference cell made and calibrated to AM 1.5(G) at NREL. The distance between the sample and the light source was approximately 20 cm. The illumination spot size was 4 cm in diameter, and the intensity fluctuated $\pm$10% over the illuminated area. Since the reference cell and sample size area are much smaller ($\sim$0.10 cm^2) than the illuminated area, it was important to match the position of the sample with that of the reference cell measurement. Experiments where the reference cell was used to gauge light intensity are denoted "AM1.5" illumination. The measurements were taken in a three-electrode configuration using a

TABLE 1: Epilayer Thickness, Direct Transition Band Gap Energy, Composition, and As:N Ratio (percentages are atomic percentage of group V elements)

sample	epilayer thickness (μm)	band gap ($\pm$0.01 eV)	%As	%P	%N	*y*:*x*
GaAsPN (2.7% N)	2	1.88	9.9	87.4	2.7	3.7
GaAsPN (3.6% N)	1	1.76	19.5	76.9	3.6	5.4
GaAsPN (4.3% N)	2	1.73	19.5	76.2	4.3	4.5

platinum counter electrode and a SSC reference electrode. The cell itself has a flat borosilicate glass window, three ground glass ports for the electrodes, and a volume of ~40 mL. The acidic and basic solutions were made from reagent-grade J. T. Baker concentrated H_2SO_4 and solid KOH. The solutions were prepared with 18 MΩ-cm water. The buffers used were colorless Hydrion buffers ranging from pH 2 to 12.

Open-circuit potentials of unplatinized electrodes were measured in a three-electrode cell using the Solartron SI 1287. Illumination was provided from the fiber optic illuminator; full intensity varied between 800 and 1200 mW/cm^2.

The Solartron SI 1287 was also used for $J-t$ testing of platinum-treated electrodes with Corrware software. Measurements were taken using the two-electrode configuration (reference and counter leads shorted) with the working electrode potentiostated at −2 V vs a platinum black counter electrode. The light source was the fiber optic illuminator. All measurements were made under 1 sun illumination.

Mott−Schottky (M−S) data was collected using the SI 1287 potentiostat in conjunction with a Solartron SI 1260 Impedance/Gain-Phase Analyzer. Data was recorded using the SAI program Zplot and viewed on SAI's Zview software. The measurements were made in a cell using the three-electrode configuration described above. The AC signal amplitude was 7 mV rms and had a range of frequencies between 100 Hz and 20 kHz. The DC ramping potential scanned at 5 mV/s, and data points were sampled at a collection frequency of 5 s/point. The potential range of the DC scan was electrode, light, and solution specific. The scans began at negative potentials, went to a more positive pivot just shy of open circuit, and then back to the starting potential. Electrodes were soaked for at least 1 h prior to analysis to allow the surface to equilibrate with the solution. The light source was the fiber optic illuminator adjusted using the readout from the thermopile power meter. A simple series RC circuit model was used for all analysis.

The electrodes were etched in reagent-grade concentrated sulfuric acid (J. T. Baker) prior to platinum surface treatments. Plating took place in a 50 mL beaker of stirred 0.0195 M H_2PtCl_6 (Aldrich) in 2 M HCl (J. T. Baker). A two-electrode cell with a a platinum foil (~2.5 cm^2) counter electrode was used, and cathodic current proportional to the electrode surface area was applied for 0.5 s followed by 2.0 s with no current. The galvanic square wave was cycled 20 times, yielding a cathodic plating charge density of 10 mC/cm^2, which was found to be the optimal amount to catalyze hydrogen evolution on p-Si photocathodes.[14] The intent of cycling the potential was to deposit platinum islands on the electrode surface. The fiber optic illuminator was used at an intensity of 50 mW/cm^2 to augment minority carriers (electrons) at the interface. No bubbles were observed during the GaPN plating procedure. The resulting platinum treatment was not noticeable to the unaided eye.

Photocathode durability analysis was a two-electrode, 24-h galvanostatic test run in 3 M sulfuric acid with the surfactant Triton X-100. This electrolyte was chosen because the electrodes evidenced higher stability from the potentiodynamic analysis. A cathodic current density of 5 mA/cm^2 was maintained at the platinized semiconductor, and bubbles evolved at both the working and the platinum black (~2.5 cm^2) counter electrode. A DC-powered 250-W tungsten−halogen Oriel model 66183 lamp provided steady illumination, and a water filter blocked the IR radiation and minimized PEC cell heating. Illumination was attenuated to AM1.5, as determined with the reference cell, using a Melles Griot neutral density filter. Solutions were saved for ICP-MS elemental analysis.

Atomic force microscopy images were obtained with a nanoSurf sensor operating in noncontact mode using nanoSurf Dynamic Force Microscopy software. The silicon tips were Nanosensors-PPP-NCLR-20, with 10−15 μm heights and a 7 nm radius.

The electrodes were dissembled, and surface profilometry of the tested semiconductor samples was accomplished with an Alpha Step 500 surface profiler. The profiles were carried out by starting with the stylus on a masked and therefore flat part of the surface and dragged 2 mm from the starting point (~0.5 mm from pit edge) into the area exposed to solution. Twelve scans were taken for each rectangular chip, three from each side. The average etch depth is the arithmetic mean of the 12 scans. The 2 mm scans took 10 s to complete.

Results and Discussion

Visual Surface Analysis. Magnified photographs of the as-grown $GaAs_yP_{1-x-y}N_x$ epilayers showed electrode surfaces replete with defects most likely due to a lattice mismatch with the substrate because none of the sample compositions met the exact lattice match condition of $y = 4.7x$. The sample with 3.6% N had by far the most observable defects in the GaAsPN material set (Figure 1a). Another possible factor contributing to defects could be carbon and hydrogen contamination that is inherent in these MOCVD-grown materials.[12] For the GaPN epilayers, surfaces with higher nitrogen concentrations were again expected to contain more defects because of the lattice mismatch with the GaP substrate. At less than 1.6% nitrogen, the surfaces looked smooth and had mirror-like specular reflection. Photomicroscopy revealed point defects for these low-nitrogen content materials similar to those observed on GaAsPN samples. Samples with nitrogen content higher than 1.6% had microscopic crosshatches and other defects that were obvious even without magnification (Figure 1b). For these samples the number and severity of defects observed with photomicroscopy generally increased with nitrogen content.

All epilayers had the zinc blend structure of the GaP substrates on which they were deposited as determined by XRD.[15−17] High-magnification SEM analyses depicted a perfect, flat surface for all samples, even those that exhibited crosshatches in optical microscopic analysis.

Band Gap. Photocurrent spectroscopy was used to determine the band gap energy and transition type.[18] The presence of a linear section in a plot of normalized photocurrent squared vs photon energy was taken to be indicative of a direct electronic transition. The band gap was found to be direct in all compositions of GaPN and GaAsPN tested. The direct band gap is a desirable attribute and agrees with theoretical predictions and experimental results of others for III−V nitride materials.[5] The compositions were estimated from XRD lattice measurements and solving a bowing equation using band gap results.

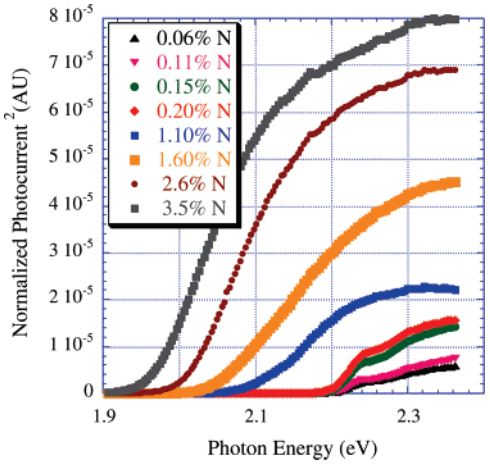

Figure 2. Direct transition photocurrent spectroscopy results for various nitrogen compositions of GaPN.

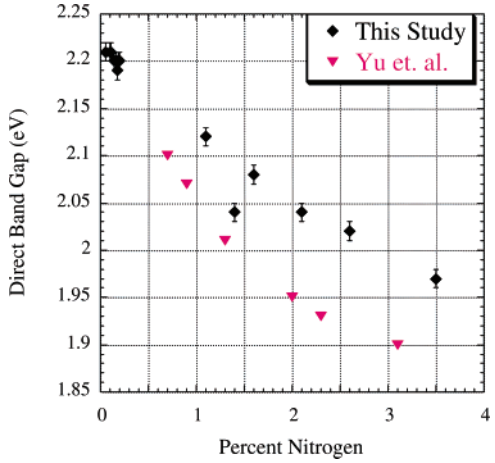

Figure 3. Direct band gap energy vs percent (group V) nitrogen. Error bars due to the band pass of the monochromator.

The measured band gap energies for the GaAsPN samples are listed in Table 1 along with the sample compositions and y:x ratio in $GaAs_yP_{1-x-y}N_x$ (y:x = 4.7:1 for lattice matching).

The absence of an indirect transition in $GaP_{.9994}N_{.0006}$ indicates that the crossover from indirect to direct occurs significantly below the 0.26% theoretically predicted.[19] That the electronic properties are affected by incorporation of roughly 1 nitrogen atom for every 3333 atoms is a testament to the considerable transformational influence of nitrogen. The effect of increasing nitrogen concentration on transition character and energy is discernible from plots of normalized photocurrent squared vs photon energy (Figure 2). Additional nitrogen causes a biphasic "direct-like" transition to become a continuous direct transition at lower energy. Our data on the direct transition band gap energy of GaPN vs percent composition (atom % of group V) along with data from Yu et al.[5] is shown in Figure 3. The data illustrate nitrogen-induced band gap bowing in GaP.

An indirect transition (square root of normalized photocurrent plotted vs photon energy) was found for both GaP and GaAsP occurring at 2.20 and 2.09 eV, respectively.

Conductivity Type, Flatband Potential, and Band Edge Positions. It is important to determine whether the conductivity of these nominally undoped samples is n- or p-type. The conductivity behavior establishes the energetic requirement for photoelectrolysis as the type determines which reaction occurs at the surface of the photoelectrode. p-type behavior means that for spontaneous water splitting the flatband potential (V_{fb}) of the photocathodes must be more positive of the oxygen evolution potential. For photoelectrolysis, p-type conductivity is preferred because it provides some cathodic protection against oxidation of the electrode material.

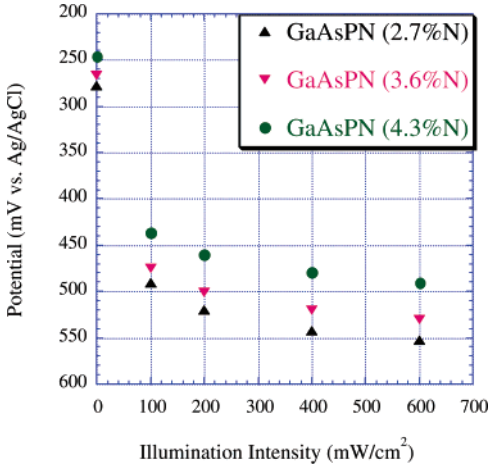

Figure 4. Open-circuit potential as a function of illumination intensity in 3 M H_2SO_4.

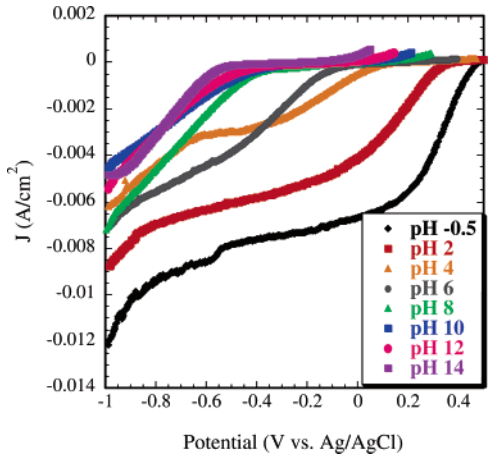

Figure 5. Illuminated (AM1.5) $J-V$ curves for platinized GaPN (1.4% N) in 3 M H_2SO_4 (pH −0.5), KOH (pH 14), and intermediate buffered solutions. All electrolytes contained the surfactant Triton X-100 to facilitate bubble evolution.

Current density−potential ($J-V$) plots can provide information on conductivity type and indicated that these undoped samples were p-type as evidenced by cathodic photocurrents at negative potentials.

Conductivity type and V_{fb} can also be established from dark and light open-circuit potential (OCP) measurements. Illuminating an electrode held at open-circuit conditions results in a flattening of the band bending at the semiconductor/electrolyte interface, shifting the Fermi level of a p-type material to more positive potentials or an n-type material to more negative potentials. If the illumination is sufficiently intense, all band bending at the junction will be removed and the resulting potential is the V_{fb}.[20]

Open-circuit measurements of As-containing samples in sulfuric acid electrolyte are plotted vs illumination intensity in Figure 4. The potential under intense illumination in 3 M sulfuric acid was found to be stable over a 30-h measurement period. The positive voltage shift in OCP upon illumination indicates that these samples, though grown undoped, exhibit p-type behavior. Note the change in the open-circuit potential with light intensity; ideally, the potential should flatten out with high light

TABLE 2: Flatband Potentials (V vs Ag/AgCl) from Various Methods Along with the Minimum V_{fb} Necessary for Photoelectrolysis (acid electrolyte was 3 M H_2SO_4 and KOH was 1 M)

method	PC onset		illuminated OCP		illuminated M−S	
electrolyte	acid	KOH	acid	KOH	acid	KOH
Vfb needed	1.3	0.53	1.3	0.53	1.3	0.53
GaAsPN (2.7% N)	0.35	−0.82	0.55	−0.08	0.23	−1.1
GaAsPN (3.6% N)	0.14	−0.91	0.53	−0.09	−0.10	−1.1
GaAsPN (4.3% N)	0.22	−0.94	0.49	−0.11	−0.05	−0.94

intensity and that would be considered the flatband potential. The GaPN samples exhibited similar behavior.

The conductivity type is also revealed by Mott−Schottky (M−S) analysis. In a p-type semiconductor the space charge region is populated by negative charges and an M−S plot will slope downward toward more positive potentials. The opposite is true for n-type materials. M−S plots for the As-containing samples had the characteristics representative of p-type electrode material.

For GaPN samples, interpretation of Mott−Schottky results was more complicated. The response for electrodes with less than 0.17% nitrogen was nonideal, but the trend in the slopes indicated p-type conductivity. At higher nitrogen compositions the M−S response was indicative of a p-type material in darkness and under illumination. This is opposite of the behavior observed in undoped InN and GaN grown by hydride vapor-phase epitaxy where chopped-light $I-V$ curves indicated n-type conductivity with an electron density of 7×10^{16} cm^{-3}.[21] This intrinsic n-type behavior was attributed to nitrogen vacancies that resulted in electron donation to the conduction band. The magnitude of the M−S slope in our GaPN samples was reduced upon illumination for most electrodes, indicative of p-type photodoping because dopant density is inversely proportional to M−S slope. The measured hole doping density typically increased by an order of magnitude upon illumination to values on the order of 1×10^{17} cm^{-3}.

Photodoping is a phenomenon common to several nitride semiconductors where above band gap illumination results in excess carriers, holes in most cases.[21−23] Carbon impurities from MOCVD growth can occupy phosphorus (or nitrogen) sites and induce deep acceptor states where electrons are trapped by the ground state of neutral carbon.[22] These electron trap states are populated by photoionization and change the material's conductivity.[24] The trap states have an energy barrier that the electrons must overcome to escape to the valence band. The same phenomenon has also been observed in the chalcogenides CdTe and CI(G)S.[25]

The precise origin of the trap states is under discussion with several trapping mechanisms considered. For GaN, in addition to carbon impurities, random potential fluctuations due to stoichiometry disorder,[23] nitrogen and gallium anti-sites and vacancies, and AX and DX centers are a few of the trap sources invoked.[26]

Photodoping is also called persistent photoconductivity (PPC) in the literature because the light-induced free carrier concentration change lasts long after the illumination source is removed,[27] and the persistent nature of the photoconductivity is more dramatic at lower temperatures.[28] PPC was not observed in these samples where removing the light restored the original unilluminated M−S response. GaN materials that exhibit PPC also have a below band edge (i.e., not a band-to-band transition) photoluminescence known as a yellow band. The yellow luminescence and PPC are related and attributed to an intrinsic defect. According to Reddy et al., this defect is independent of the growth technique,[24] indicating carbon contamination is not the exclusive origin. Deep level trapping states encourage recombination and compromise the electronic properties of the material by drastically reducing minority carrier lifetimes.[29] Another possible cause of photodoping could be a large difference between the mobilities of the two carriers. If the effective mass of holes is larger, which is typically the case in semiconductors, electrons will be generated and swept out of the material more quickly than holes. The space charge region would be hole enriched and therefore p-type.

The GaPN sample with 0.20% N had a complete inversion of behavior with illumination going from n-type in the dark to p-type under illumination, indicating the sample was likely compensated. A compensated semiconductor has both n- and p-type dopants. Compensated behavior has been observed in carbon-doped GaN where the nominally undoped material was n-type ($\sim 10^{16}$ cm^{-3}). The behavior was attributed to carbon in nitrogen sites that induces deep acceptor states that compensate for the residual donor states.[22] The change in sign of the M−S slope upon illumination indicates a similar phenomenon is occurring in this one particular sample run.

The flatband potential can be determined from $J-V$ analysis. Photocurrent onset is found by plotting photocurrent squared vs potential and extrapolating the linear portion to the x axis, which (in the ideal case) is the flatband potential.[18] Illuminated $J-V$ curves across the pH range (Figure 5) showed a negative shift in V_{fb} with increasing OH^- concentration in the electrolyte.

The flatband potential determined by OCP measurements for GaAsPN (3.6% N) and p-GaP epilayers grown on p-GaP for a range of solution pH's showed a Nernstian dependence of V_{fb} on pH that usually indicates [H^+]-dependent deprotonation and protonation of surface hydroxyl and oxide species commonly seen in III−V semiconductor electrolyte interfaces.

Knowledge of the band gap, flatband potential, and apparent (photo)doping density allowed the potential of the valence and conduction bands at the interface to be determined. The p-GaP data indicated the band edges for our samples are significantly more negative than the 300 mV cathodic offset reported in the literature.[4] Addition of arsenic and nitrogen appears to shift the V_{fb} slightly negative compared to pure GaP. The GaAsPN V_{fb} values obtained from the three methods of analysis as well as the flatband potential needed for spontaneous photoelectrolysis are given in Table 2. Since a large positive shift is required to achieve appropriate band alignment, it appears unlikely that any GaAsPN composition would have suitable interfacial energetics.

For the GaPN material set, the flatband potentials determined by the onset of cathodic photocurrent were all too negative of the water oxidation potential by nearly 1 V in many cases. The OCP-determined flatband potentials were closer and fell within 300−500 mV of the required potential. Nevertheless, V_{fb} values from OCP analysis (Figure 6a) were still too negative, thus rendering all GaPN compositions evaluated incapable of direct photoelectrolysis. The polarity of the mismatch of the GaPN epilayers is the same as most III−V's, the flatband potential is too negative, and consequently the hole has insufficient oxidizing power to drive the oxygen evolution half-reaction.

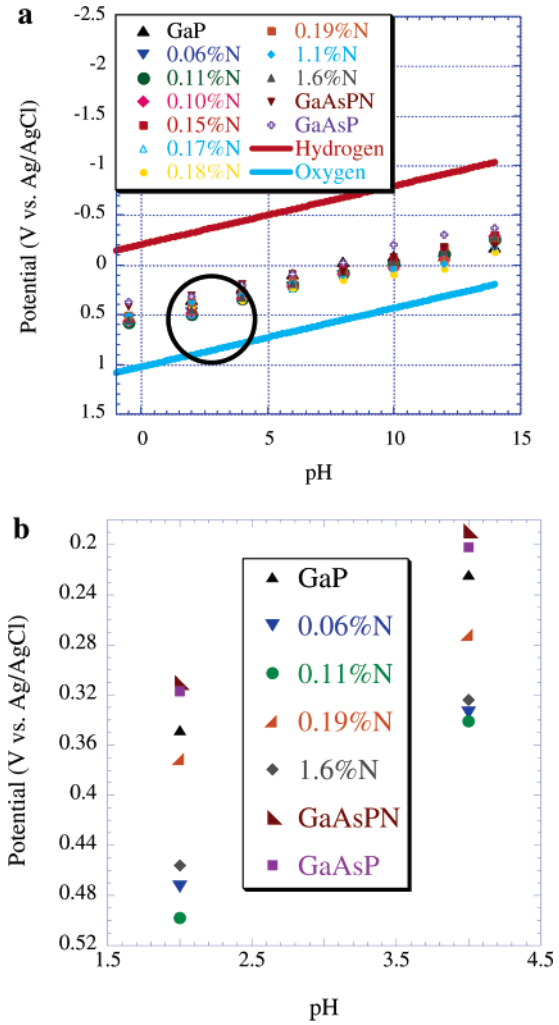

Figure 6. Illuminated OCP determined V_{fb}. (a) All of the compositions examined and their relationship to the water splitting potentials. (b) Close-up view of a limited set of data from within the circle.

The relative relationships evident in the bottom plot of Figure 6b were also observed in the V_{fb} values determined from photocurrent onset. Both sets of data indicate that nitrogen addition results in flatband potentials with values more positive than that of GaP. The relationship appears to be nonlinear with a maximum effect at a low nitrogen composition (Figure 6b). This is most likely due to the increase in defects with additional nitrogen as the lattice constant of the epilayer moves away from lattice matching with the substrate. Recombination at defect sites can influence OCP and photocurrent onset flatband measurements by preventing the band from flattening in one case and delaying the photocurrent onset in the other. An alternate explanation would be that initially nitrogen shifts both bands toward the overlap condition but subsequent nitrogen reduces the band gap by moving the valence band toward the vacuum. It is assumed that at the nitrogen-rich end of the compositional spectrum the bands will have to migrate back down to fulfill the overlap condition observed for pure GaN.[3]

As determined from OCP and photocurrent onset, addition of arsenic to the GaP lattice shifted the flatband potential to more negative values. This negative trend was apparently more influential than the opposing influence of nitrogen in the quaternary GaAsPN material (Figure 6b). Although the GaAsPN materials have higher nitrogen content than the GaPN epilayers, the OCP is more negative likely due to the large amounts of As. The effect of arsenic incorporation on OCP prevents

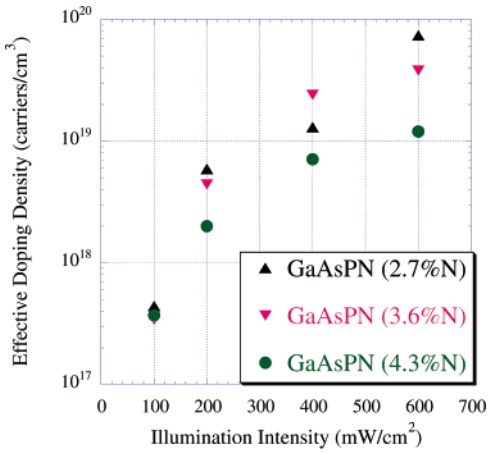

Figure 7. Increased N_A with illumination from M−S slopes taken on electrodes in 1 M KOH with AC frequency 3 kHz.

TABLE 3: Fermi Level Position (ΔE) with Respect to Valence Band Energy[a]

sample	acceptor density (cm^{-3})	Fermi level (eV)
GaAsPN (2.7% N)	7.8E+16	0.13
GaAsPN (3.6% N)	9.4E+16	0.12
GaAsPN (4.3% N)	1.9E+17	0.10

[a] Calculated apparent doping density from 2 sun illuminated, 20 kHz, basic solution M−S plots.

extrapolating nitride's effect from GaPN data points to the higher nitrided GaAsPN epilayers where another variable is introduced. Moreover, in the two GaAsPN samples that have the same As content, additional nitrogen shifts the OCP negative (Figure 4). This is contrary to the relationship observed in nitrogen-lean GaPN. It is a promising result that small amounts of nitrogen appear to shift the flatband potential in the right direction in the absence of arsenic. However, it is doubtful that the magnitude of shift necessary for band overlap could be realized in the nitrogen compositions currently attainable for GaPN.

While the flatband potential value should be independent of the technique used to determine it, the lack of congruence of values determined by the various analyses for these samples can be rationalized by the nonideality exhibited by these samples.

The V_{fb} derived from $J-V$ analysis can have a systematic error from reaction overpotential, an additional potential beyond the E for a reaction that must be supplied to overcome kinetic limitations. For p-type, systematic error due to overpotential gives V_{fb} values that are too negative. Overpotentials can be reduced by depositing a catalyst on the electrode surface, so in this study, platinum was used as the catalyst for hydrogen evolution. However, the photocurrent onset potential was only moderately shifted on platinized electrodes.

OCP-determined V_{fb} values can be complicated by imperfect materials because defect sites provide recombination centers that can prevent the bands from completely flattening. In this case for p-type, V_{fb} determined experimentally is systemically negative of the true V_{fb}. Since these samples have visible defects, this complicating factor most likely affected the flatband values determined using this method.

In the ideal case M−S analysis is frequency independent. Surface state capacitance can contribute to the signal and give a frequency dependence to the M−S results. Frequency-dependent plots can result in unrealistic values obtained for V_{fb} and acceptor densities (N_A). These materials had M−S plots that were frequency dependent to varying degrees.

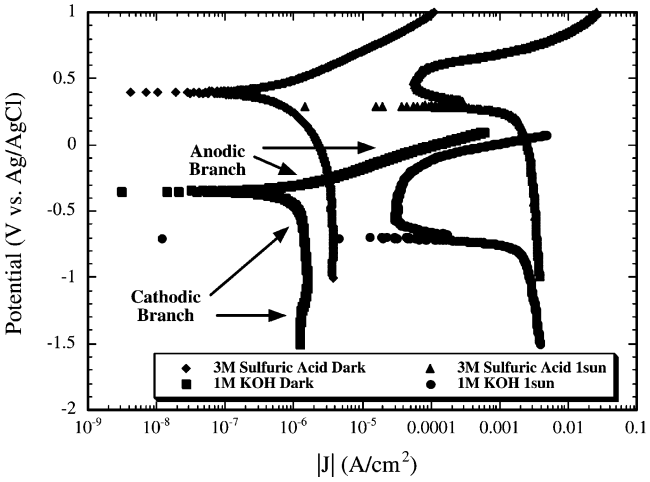

Figure 8. Potentiodynamic analysis of platinized GaAsPN (2.7% N).

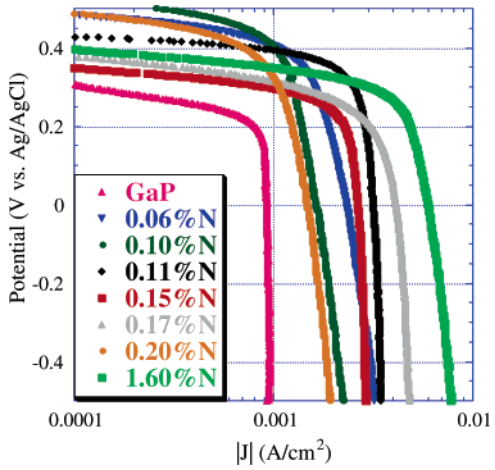

Figure 9. Cathodic branches of potentiodynamic analysis of GaP and GaPN with varying nitride content in 3 M H_2SO_4 with the surfactant Triton X-100. The electrodes were platinized and illuminated (AM1.5).

Figure 7 illustrates the phenomenon of photodoping where N_A increased with illumination. These values ranged from 10^{16} to 10^{21} cm^{-3} and were calculated using slopes of M−S plots made from electrodes under various states of illumination assuming a relative dielectric of 10. All the V_{fb} values determined by M−S under illumination were too negative to split water by about 1 V on average.

For p-type semiconductors the Fermi level lies just above the top of valence band edge energy. The exact energy of the Fermi level can be found if the dopant density and valence band effective density of states, N_V, are known using the equation

$$E_V - E_F = k_B T \ln\left(\frac{N_A}{N_V}\right) \quad (1)$$

for p-type semiconductors.[30] N_V can be found using the relation

$$N_V = 2\left(\frac{2\pi m_h^* k_B T}{h^2}\right) \quad (2)$$

where h is Planck's constant and m_h^* is the effective hole mass. Assuming m_h^* for this quaternary alloy is between 0.47 m_e in GaAs and 0.60 m_e in GaP and GaN, N_V at 300 K will fall between 8.7×10^{18} and 1.2×10^{19} cm^{-3}. Some of the data points in Figure 7 from low-frequency data indicate a carrier density greater than the effective density of states. The doping

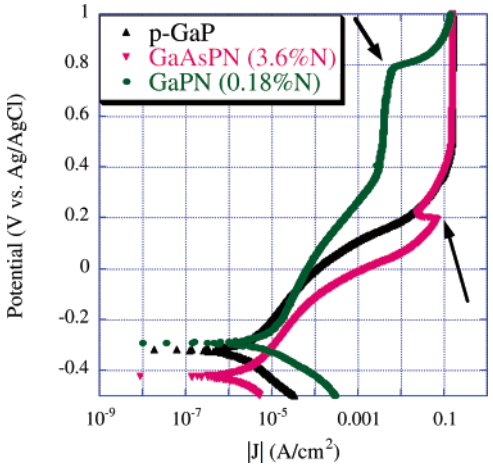

Figure 10. Illuminated (1 sun) KOH potentiodynamic plot exhibiting total epilayer dissolution.

TABLE 4: Etch Depth through Nominal 1 μm Epilayer into GaP Substrate for Electrodes Subjected to Potentiodynamic Analysis

sample	electrolyte	etch depth (μm)
pGaP	H_2SO_4	6.86
GaPN (0.18% N)	H_2SO_4	4.16
GaAsPN (3.6% N)	H_2SO_4	7.41
p-GaP	KOH	23.43
GaPN (0.18% N)	KOH	12.54
GaAsPN (3.6% N)	KOH	24.31

densities found from higher frequency (20 kHz) M−S plots are roughly 2 orders of magnitude lower and thus more believable. Higher frequency M−S analyses are better at screening out surface state contributions to capacitance that can swamp the depletion layer capacitance at lower frequencies. The high-frequency data were collected at a single illumination intensity and thus could not be used to calculate Fermi level positions as a function of illumination. The calculated Fermi levels from 200 mW/cm^2 illuminated, high-frequency M−S plot slopes with an assumed $N_V = 1.0 \times 10^{19}$ cm^{-3} appear in Table 3. Photodoping density from Table 3 indicates a direct correlation with nitrogen content. The band gap of these materials as well as the location of the Fermi level, within 150 eV of the valence band under moderate illumination, means band alignment would be achieved with a V_{fb} slightly positive of the oxygen evolution potential.

Material Stability. Comparing potentiodynamic curves in light and dark showed that photocorrosion is a problem for these materials. For ideal p-type material, the dark and illuminated anodic branches should overlap and be at current densities well below the illuminated cathodic branch. For the GaAsPN materials the anodic branch was nearly horizontal in a plot of potential vs log current density, indicating little resistance to anodic corrosion (Figure 8). In similar studies on $GaInP_2$ the anodic branch was nearly vertical and at a lower current density than the cathodic branch.[31] This suggests that GaAsPN is not as stable as $GaInP_2$, which itself has stability issues. The current density for platinized samples was higher than that of the untreated electrodes for both branches of the potentiodynamic curve. Clearly the platinum-catalyzed hydrogen production in the cathodic branch, whether it also catalyzed semiconductor oxidation in the anodic branch or catalyzed oxygen, is unknown at this time. Limiting photocurrent densities were equivalent in acid and base over the whole range of (normalized) potentials. All of the features described above can be seen in the potentiodynamic scans of platinum-treated GaAsPN (2.7% N) (Figure

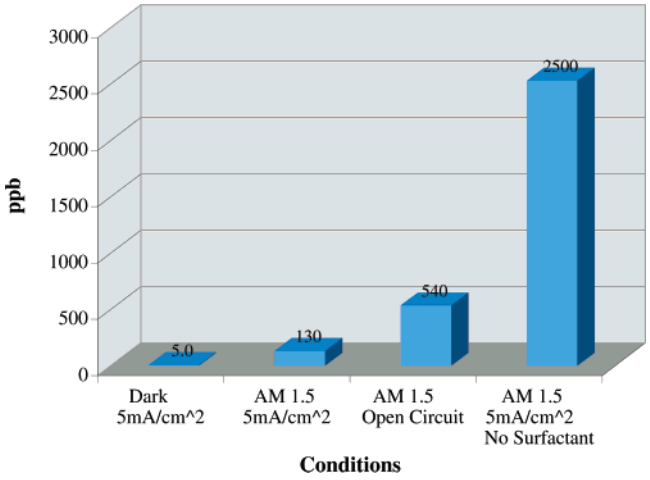

Figure 11. ICP−MS detected 24-h durability solution compositions for a variety of GaPN (2.1% N) sample conditions.

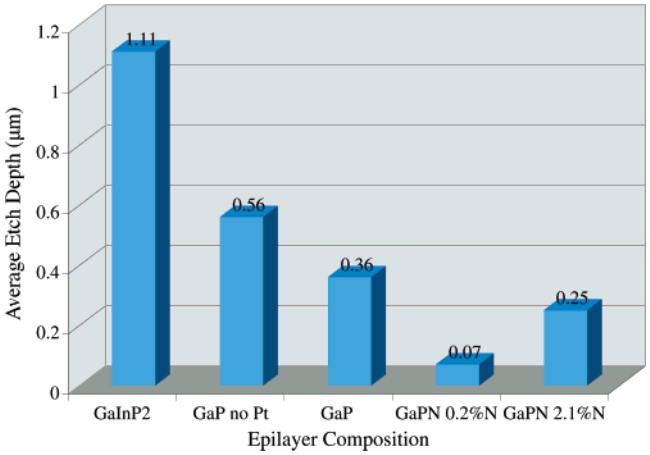

Figure 12. Subset of etch depth data that illustrates overall stability trend and effect of platinum surface treatment.

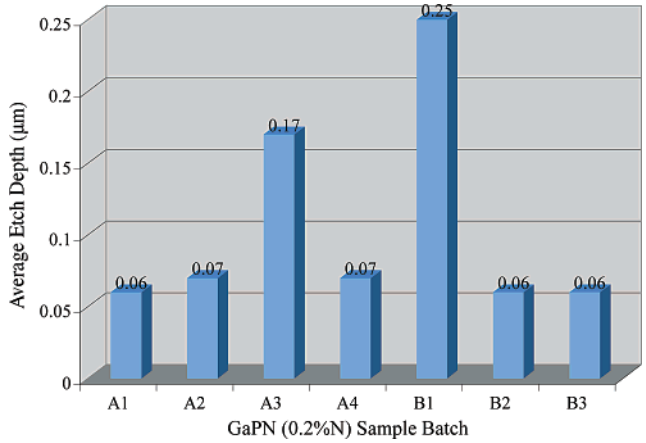

Figure 13. GaPN (0.2% N) 24-h durability run etch depth variation between multiple replicates from two batches.

8). Examination of the cathodic branches of illuminated potentiodynamic plots (Figure 9) reveals there is not a linear correlation between nitrogen content and photocurrent magnitude.

Illuminated potentiodynamic analysis of the 1 μm thick GaAsPN (3.6% N) in KOH shows an abrupt change in current density in the anodic branch. This appears to be the point in the experiment where the epilayer has been completely stripped off, exposing the GaP substrate. This conclusion is more obvious when it is compared with results from 1 μm epilayers of GaP and arsenic-free GaPN (0.18% N) on GaP substrates (Figure 10). The higher anodic current density of GaAsPN indicates that it is less stable than GaP until it is exhausted, denoted by the arrow on the plot, and returns to the GaP baseline corrosion current. The GaPN material at first is more resistant to anodic dissolution until it too is completely stripped (arrow) and current density traces the GaP baseline. After the above analysis, the electrodes were disassembled and etch depth was determined with profilometry. The etch depths given in Table 4 tell the same story as the potentiodynamic plots. The order of material stability from least to greatest is GaAsPN < GaP < GaPN. Acidic solutions appear to be the less corrosive environment, which is in agreement with previous GaP observations.[4]

Measurement of operational stability can be deduced from illuminated current density (J) vs time (t) plots, where a constant cathodic photocurrent density over the duration of the run would indicate the electrode is resistant to corrosion reactions that lead to photocurrent decay. However, for a more quantitative assessment of the material durability, we imposed a constant current of -5 mA/cm^2 for 24 h under AM 1.5 illumination intensity in 3 M H_2SO_4 and then used inductively coupled plasma mass spectrometry (ICP-MS) analysis of the resulting solutions and measurement of the epilayer etch depths for the disassembled electrodes. This allowed corrosion rates to be assessed and compared to electrodes that had passed the same charge density.

A simple relationship between nitrogen composition and material stability was not noted in the ICP-MS results. Generally, nitrides had less gallium in solution than solutions from similarly treated GaP. The durability analysis solution for a $GaInP_2$/GaAs tandem electrode that passed equivalent charge contained 10 times more gallium content than a solution from a typical nitride material despite having a lower gallium ratio in the epilayer ($GaInP_2$ is a mixed group III). Changing specific variables in the durability analysis led to corrosion results that validated some expected predictions. The validations are rationalized from the results plotted in Figure 11. The concentration of gallium was normalized to account for variation in surface area and solution volume and is plotted for the same sample compositions run under a variety of conditions.

The first observation is that illumination accelerates corrosion. This is evident in the high [Ga] from the illuminated electrodes relative to the dark sample. The explanation is that illumination promotes an electron from a bonding orbital to an antibonding orbital, leaving species at the interface prone to chemical attack and dissolution; this does not occur in the absence of illumination. In the absence of light, electrons are supplied through the bulk by a potentiostat, leaving bonds among surface species intact and thus more stable. The presence of a hole in the surface bond means that one of the electrons in the bonding orbital has been removed, leaving a positively charged surface species that can more easily react with the solution.[32] Memming states that because valence bonds are broken, most corrosion steps occur by hole consumption via the valence band.[33] Accordingly, anodic dissolution occurs on p-type in the dark and n-type in the light, which underscores the importance of conductivity type in curtailing corrosion. As solar energy conversion is the intended use of these materials, they must be able to persist in an illuminated environment.

The second observation from Figure 11 concerns cathodic current flow offering protection from corrosion. The cathodic protection is evident from the low [Ga] in solutions from normal and dark runs compared to the sample that was illuminated but held at open circuit. This effect is likewise related to electron populations in bonding orbitals. Under cathodic current flow,

TABLE 5: MOCVD Growth Conditions for a Variety of GaPN and GaP Epilayers[a]

run no.	DMH (sccm)	T_g (°C)	%N XRD	%N SIMS	[H] (ppm)	[C] (ppm)	[O] (ppm)
1	80	700	2.10	1.38	44	7	8
2	10	700	0.20	0.16	49	3	5
3	0	700	0	0	42	4	9
4	10	750	<0.05	0.03	60	11	18
5	10	700	0.20	0.24	19	3	4
6	40	700	1.40	1.01	10	6	5
7	0	700	0	0	9	6	13

[a] XRD and SIMS determined nitrogen is percentage of group V elements. Contaminants are reported as atomic concentration.

bonding orbital electrons in surface species are replenished by photoelectrons forced to the surface by the electric field in the depletion region. Open-circuit condition does not force this movement of charges and thus restricts this mechanism of protecting the surface. Fortunately, in regard to current flow, the operating conditions for hydrogen production also favor electrode stability.

The final observation from ICP-MS data is that addition of surfactant to the electrolyte significantly diminishes corrosion. Previous researchers found that the same surfactant inhibited etching on Si (111) and (100) surfaces,[34] which they attribute to formation of a self-assembled micellar layer at the semiconductor/electrolyte interface. Additionally, facile bubble evolution likely precludes problems associated with adherence of hydrogen gas bubbles to the semiconductor surface. Electron transfer to the solution is only possible where the surface is in contact with the solution, and since we are passing a constant current, the aggregate current must be maintained by increasing the charge flow through the areas that are in contact with the electrolyte. It is assumed that the resulting large local variations in current density contribute to surface instability. Bubble formation is also implicated in creating lenses that focus incoming radiation, which produces "hot spots". The resulting nonuniform illumination causes local variations in surface potential, which may also favor decomposition. The surfactant lowers the solution surface tension, reducing the bubble size, thus preserving the intimate electrolyte contact at the semiconductor/electrolyte interface.

Profilometry measurements made on disassembled electrodes were able to determine the etching depth that occurred during durability analysis. All of the samples that contained nitrogen had a lip at the perimeter of the exposed area and displayed gradual etching that increased toward the center of the chip; material dissolution was less than the 1 μm thick epilayer. For the $GaInP_2$/GaAs tandem materials, the etching left a nearly vertical wall at the exposed/masked border, and the samples were etched about 1 μm into their 4.5 μm thick epilayers (2 μm in a couple instances). The nitride etch depth did not have a simple dependence on nitrogen content, but the depth and shape of the profiles clearly indicate that the nitride materials provide some additional resistance against corrosion.

A subset of average etch depths (Figure 12) demonstrates the general stability trend observed with $GaInP_2$ being the least stable, nitrides being the most stable, and GaP falling somewhere in between. The results for GaPN epilayers with 0.2% N and 2.1% N indicate that lattice matching is an important consideration in minimizing corrosion. The 2.1% nitrogen sample would be expected to have a high number of defects due to large lattice mismatch. The results show that this epilayer was more prone to corrosion than the nearly lattice-matched 0.2% N. Even though most of the nitrides showed little etching compared to their counterparts, any degree of etching will limit lifetime. The magnitude of the etching that occurred over the 24-h run can be used to estimate material lifetime. The 0.06 μm etching represents nearly 20 days of stability for 1 μm films. This is a significant improvement over the 20-h stability observed previously in the $GaInP_2$/GaAs material.

Figure 12 also corroborates the idea that platinum surface treatment can enhance photoelectrode stability. This has been observed by many researchers in the past and attributed to the lower overpotential of hydrogen evolution from platinum. The platinum catalyst improves the kinetics of the hydrogen reaction, making it more competitive with the thermodynamically favored corrosion reactions.[4] On the other hand, the platinum islands are also effective hole traps.[35] Photogenerated holes are collected from the valence band at the near surface, where they are strong oxidants and could contribute to corrosion. However, it is more likely they are trapped in platinum where they recombine with electrons. The recombination mechanism thus described is desirable in mitigating corrosion, but excessive recombination curtails efficiency. In summary, platinizing photoelectrodes has been proven to catalyze the hydrogen evolution reaction resulting in higher efficiency compared to bare electrodes.

Reproducibility of profilometry-aided durability analysis was probed by examining four samples from one run (A) and three from another (B) that were grown using the same MOCVD recipe (nominally 0.2% nitrogen GaPN grown on p-GaP). Differences between the two might be attributed to variability involved in sample growth. There was fairly good agreement from electrodes made from A and excellent reproducibility in all but one of them (Figure 13). The same observation holds true for B. If the outlier is thrown out from each sample, the resulting etch depths are nearly identical. The two samples that demonstrated poor stability could have had inherent surface defects that accelerated the corrosion reactions.

Atomic force microscopy (AFM) was used to make more detailed, qualitative observations of surfaces. By comparing materials both before and after analysis, the degree of surface change could be correlated to corrosion when operated in an electrochemical cell.

Nitride epilayers had a lower degree of surface alteration (roughness) compared to GaP as a result of $J-t$ analysis. All electrode surfaces were relatively flat prior to analysis. The postanalysis surface of GaP had surface features that were greater in number and scale than those on GaPN surfaces. The samples with the lowest nitrogen content had the highest apparent stability of all the materials. The change in surface topography was more dramatic when basic solution was the electrolyte.

Auger electron spectroscopy (AES) was unable to detect nitrogen in these materials. AES profiles did, however, reveal surfaces rich in carbon and oxygen. Secondary-ion mass spectrometry (SIMS) was able to detect nitrogen in very dilute amounts. The SIMS resolution allowed comparison to nitrogen content derived from XRD data (Table 5). There was general agreement in nitrogen content from XRD and SIMS when the same chip was used for both analyses. When the data was collected from separate pieces cleaved from the same run the results varied to a degree that indicates compositional inhomo-

geneity across the sample. SIMS was also able to track trace quantities of the impurities H, C, and O through the material bulk. The flow rate of dimethylhydrazine (DMH) and growth temperature, columns 2 and 3 of Table 5, dictate nitrogen content of the epilayer. The increased impurity concentration in run 4 is attributed to the elevated growth temperature and agrees with literature.[12]

Conclusions

On the basis of these experiments, GaAsPN does not meet the requirements for a functional single-gap water splitting photoelectrode. While the band gap is direct and energetic enough to drive the reaction, the band edges are mismatched, preventing the oxygen reaction from occurring at the counter electrode. The stability of GaAsPN photoelectrodes also appears to be poor from these studies, most likely compromised by arsenic. Arsenic is amphoteric and can dissolve in either acid or base, and any gains in stability achieved by nitrogen incorporation appear to be overridden by arsenic. Another deficiency of this material was that several of the semiconductors fractured over time, indicative of the macroscopic manifestation of the strain introduced in the material by substrate lattice mismatch. All of these attributes make the application of GaAsPN for photoelectrolysis unlikely.

Nitrogen incorporation in GaP induced a direct transition even with trace amounts of nitrogen. A band gap of ~2 eV, optimal for water splitting applications, occurs in GaPN epilayers with about 2% nitrogen. Growth of $GaP_{0.98}N_{0.02}$ by MOCVD on GaP led to defect-dominated surfaces due to the lattice mismatch between the GaPN and the GaP substrate. Even if defect-free 2 eV band-gap GaPN (2% N) materials can be grown, our measurement of the band edges showed that they are too negative to drive water splitting. While there was some variation in flatband potentials determined from OCP and photocurrent onset, most samples had a mismatch of at least 500 mV. Addition of nitrogen appears to shift the band edges toward the direction needed but nowhere near the magnitude necessary to achieve overlap. The interfacial energetics of GaP were found to be less favorable for water splitting than reported in the literature.[4]

A promising conclusion is that nitrogen has an obvious influence on enhancing the material's resistance to chemical attack by the electrolyte. The passivating effect is obvious primarily at very low concentrations of nitrogen. Additional nitrogen degraded the stability, although the mechanism is thought to be related to surface defects from lattice mismatch and not due to nitrogen per se. In the absence of surface defects, we would expect higher corrosion resistance with increased nitrogen concentration. Higher nitrogen content samples also showed a tendency to fracture during use, which we attribute to material strain, again due to the high degree of lattice mismatch. Use of a substrate with a smaller lattice constant should allow the growth of defect-free GaPN epilayers with more nitrogen, possibly enhancing the potential for PEC water splitting.

Acknowledgment. The authors thank Sarah Kurtz for constructive advice and guidance and John Geisz for sample growth, ohmic contacts, XRD analysis, composition estimates, reference cells, and valuable feedback. ICP−MS analyses by Fredrick Luiszer at CU are appreciated. This work was conducted at the National Renewable Energy Laboratory and funded by the Department of Energy Hydrogen Program contract number NXDJ-9-29638-23.

References and Notes

(1) Kocha, S. S.; Turner, J. A. Displacement of Bandedges of $GaInP_2$ in Aqueous Electrolytes Induced by Surface Modification. *J. Electrochem. Soc.* **1995**, *142* (8), 2625−2630.

(2) Kocha, S. S.; Peterson, M. W.; Arent, D. J.; Redwing, J. M.; Tischler, M. A.; Turner, J A. Electrochemical Investigation of the Gallium Nitride-Aqueous Electrolyte Interface. *J. Electrochem. Soc.* **1995**, *142* (12), 238−240.

(3) Beach, J. D.; Collins, R. T.; Turner, J. A. Band-Edge Potentials of n-Type and p-Type GaN. *J. Electrochem. Soc.* **2003**, *150* (7), A899−A904.

(4) Ginley, D. S.; Butler, M. A. Gallium Phosphide. In *Semiconductor Electrodes: studies in physical and theoretical chemistry*; Finklea, H.O., Ed.; Elsevier: New York, 1988; Vol. 55, pp 329−372.

(5) Yu, K. M.; Shan, W.; Wu, J. Nature of the fundamental band gap in GaN_xP_{1-x} alloys. *Appl. Phys. Lett.* **2000**, *76* (22), 3251−3253.

(6) Buyanova, I. A.; Chen, W. M.; Tu, C. W. Recombination processes in N-containing III-V ternary alloys. *Solid-State Electron.* **2003**, *47*, 467−475.

(7) Biwa, G.; Yaguchi, H.; Onabe, K.; Shiraki, Y. Metalorganic vapor-phase epitaxy of $GaP_{1-x-y}As_yN_x$ quaternary alloys on GaP. *J. Cryst. Growth* **1998**, *189/190*, 485−489.

(8) Geisz, J. F. *Application of III-V Semiconductor Heterostructures to Optical Chemical Sensing, in Chemical Engineering*; University of Wisconsin: Madison, WI, 1995; p 332.

(9) Geisz, J. F.; Friedman, D. J.; Kurtz, S. GaNPAs Solar Cells Lattice-Matched to GaP. In *Proceedings of the 29th Photovoltaic Specialists Conference*, New Orleans, LA, May 20−21, 2002; IEEE: New York, 2002.

(10) Geisz, J. F.; Reedy, R. C.; Keyes, B. M.; Metzger, W. K. Unintentional carbon and hydrogen incorporation in GaNP grown by metal-organic chemical vapor deposition. *J. Cryst. Growth* **2003**, *259*, 223−231.

(11) Geisz, J. F.; Friedman, D. J. III-N-V semiconductors for solar photovoltaic applications. *Semicond. Sci. Technol.* **2002**, *17*, 769−777.

(12) Geisz, J. F.; Reedy, R. C.; Keyes, B. M.; Metzger, W. K. Unintentional Carbon and Hydrogen Incorporation in GaNP Grown by Metal-Organic chemical vapor deposition. *J. Cryst. Growth* **2003**, *259*, 223−231.

(13) Bansal, A.; Turner, J. A. Suppression of Band Edge Migration at the p-$GainP_2$/H_2O Interface under Illumination via Catalysis. *Phys. Chem. B* **2000**, *104* (28), 6591−6598.

(14) Dominey, R. N.; Lewis, N. S.; Bruce, J. A.; Bookbinder, D. C.; Wrighton, M. S. Improvement of Photoelectrochemical Hydrogen Generation by Surface Modification of p-Type Silicon Semiconductor Photocathodes. *J. Am. Chem. Soc.* **1982**, *104*, 467−482.

(15) Geisz, J. F.; Friedman, D. J.; Kurtz, S. GaNPAs Solar Cells Lattice-Matched to GaP. In 29th IEEE PV Specialists Conference, New Orleans, LA, 2002.

(16) Geisz, J. F.; Olson, J. M.; Friedman, D. J.; Jones, K. M.; Reedy, R. C.; Romero, M. J. Lattice-Matched GaNPAs-on-Silicon Tandem Solar Cells. In 31st IEEE Photovoltaics Specialists Conference and Exhibition, Lake Buena Vista, FL, 2005.

(17) Geisz, J. F.; Friedman, D. J.; McMahon, W. E.; Ptak, A. J.; Kibbler, A. E.; Olson, J. M.; Kurtz, S.; Kramer, C.; Young, M.; Duda, A.; Reedy, R. C.; Keyes, B. M.; Dippo, P.; Metzger, W. K. GaNPAs Solar Cells that Can Be Lattice-Matched to Silicon; NCPV: Denver, CO, 2003; pp 1−4.

(18) Beach, J. D. InGaN for Photoelectrochemical Water Splitting. *Applied Physics*; School of Mines: Golden, CO, 2001; p 125.

(19) Benkabou, F.; Becker, J. P.; Certier, M.; Aourag, H. Calculation of Electronic and Optical Properties of Zinc Blende $GaP_{1-x}N_x$. *Superlattices Microstruct.* **1998**, *23* (2), 453−465.

(20) Turner, J. A. Energetics of the Semiconductor-Electrolyte Interface. *J. Chem. Educ.* **1983**, *60*, 327−329.

(21) Lindgren, T.; Larsson, M.; Lindquist, S.-E. Photoelectrochemical characterisation of indium nitride and tin nitride in aqueous solution. *Sol. Energy Mater. Sol. Cells* **2002**, *73*, 377−389.

(22) Lopatiuk, O.; Osinsky, A.; Dabiran, A.; Gartsman, K.; Feldman, I.; Chernyak, L. Electron trapping effects in C- and Fe-doped GaN and AlGaN. *Solid-State Electron.* **2005**, *49*, 1662−1668.

(23) Theuwis, A.; Strubbe, K.; Depestel, L. M.; Gomes, W. P. A Photoelectrochemical Study of $In_xGa_{1-x}N$ Films. *J. Electrochem. Soc.* **2002**, *149* (5), E173−E178.

(24) Reddy, C. V.; Balakrishnan, K.; Okumura, H.; Yoshida, S. The origin of persistent photoconductivity and its relationship with yellow luminescence in molecular beam epitaxy grown undoped GaN. *Appl. Phys. Lett.* **1998**, *73* (2), 244−246.

(25) Agostinelli, G.; Dunlop, E. D.; Batzner, D. L.; Tiwari, A. N.; Nollet, P.; Burgelman, M.; Kontges, M. Light Dependent Current Transport Mechanisms in Chalcogenide Solar Cells. In *Proceedings of the Third World Conference on Photovoltaic Energy Conversion*, Osaka, Japan, May 11−18, 2003; IEEE: New York, 2003; Vol. 1, pp 356−359.

(26) Poti, B.; Passaseo, A.; Lomascolo, M.; Cingolani, R.; De Vittorio, M. Persistent photocurrent spectroscopy of GaN metal-semiconductor-

metal photodetectors on long time scale. *Appl. Phys. Lett.* **2004**, *85* (25), 6083−6085.

(27) Castaldini, A.; Cavallini, A.; Polenta, L. Deep levels and irradiation effects in n-GaN. *J. Phys.: Condens. Matter* **2000**, *12*, 10161−10167.

(28) Queisser, H. J.; Theodorou, D. E. Decay kinetics of persistent photoconductivity in semiconductors. *Phys. Rev. B* **1986**, *33* (6), 4027−4033.

(29) Queisser, H. J.; Haller, E. E. Defects in Semiconductors: Some Fatal, Some Vital. *Science* **1998**, *281*, 945−950.

(30) Green, M. A. *Solar Cells*; The University of New South Wales: Kensington, 1998; p 274.

(31) Khaselev, O.; Turner, J. A. Electrochemical Stability of p-$GaInP_2$ in Aqueous Electrolytes Toward Photoelectrochemical Water Splitting. *J. Electrochem. Soc.* **1998**, *145* (10), 3335−3339.

(32) Decker, F.; Soltz, D. A.; Cescato, L. From Photocorrosion to Photoelectrochemical Etching. *Electrochim. Acta* **1993**, *38* (1), 95−99.

(33) Memming, R. *Semiconductor Electrochemistry*; Wiley-VCH: Weinheim, 2001; p 399.

(34) Allongue, P.; Kieling, V.; Gerischer, H. Atomic Structure of Si Surfaces Etched in Triton/NaOH Solutions. *J. Phys. Chem.* **1995**, *99*, 9472−9478.

(35) Lewis, N. S. Frontiers of Research in Photoelectrochemical Solar Energy Conversion. *J. Electroanal. Chem.* **2001**, *508*, 1−10.